

Discriminating Z' from anomalous trilinear gauge coupling signatures in $e^+e^- \rightarrow W^+W^-$ at ILC with polarized beams

V. V. Andreev,^{a,*} G. Moortgat-Pick,^{b,†} P. Osland,^{c,d,‡} A. A. Pankov^{e,§} N. Paver^{f,¶}

^a*The F. Scorina Gomel State University, 246019 Gomel, Belarus*

^b*DESY FLC, Notkestrasse 85, Hamburg 22607, Germany*

^c*Department of Physics and Technology,
University of Bergen, Postboks 7803, N-5020 Bergen, Norway*

^d*CERN, CH-1211 Genève 23, Switzerland*

^e*The Abdus Salam ICTP Affiliated Centre,
Technical University of Gomel, 246746 Gomel, Belarus*

^f*University of Trieste and INFN-Trieste Section, 34100 Trieste, Italy*

arXiv:1205.0866v2 [hep-ph] 4 Sep 2012

* quarks@gsu.by

† gudrid.moortgat-pick@desy.de

‡ per.osland@ift.uib.no

§ pankov@ictp.it

¶ nello.paver@ts.infn.it

Abstract

New heavy neutral gauge bosons Z' are predicted by many models of physics beyond the Standard Model. It is quite possible that Z' s are heavy enough to lie beyond the discovery reach of the CERN Large Hadron Collider LHC, in which case only indirect signatures of Z' exchanges may emerge at future colliders, through deviations of the measured cross sections from the Standard Model predictions. We discuss in this context the foreseeable sensitivity to Z' s of W^\pm -pair production cross sections at the e^+e^- International Linear Collider (ILC), especially as regards the potential of distinguishing observable effects of the Z' from analogous ones due to competitor models with anomalous trilinear gauge couplings (AGC) that can lead to the same or similar new physics experimental signatures at the ILC. The sensitivity of the ILC for probing the Z - Z' mixing and its capability to distinguish these two new physics scenarios is substantially enhanced when the polarization of the initial beams and the produced W^\pm bosons are considered. A model independent analysis of the Z' effects in the process $e^+e^- \rightarrow W^+W^-$ allows to differentiate the full class of vector Z' models from those with anomalous trilinear gauge couplings, with one notable exception: the sequential SM (SSM)-like models can in this process not be distinguished from anomalous gauge couplings. Results of model dependent analysis of a specific Z' are expressed in terms of discovery and identification reaches on the Z - Z' mixing angle and the Z' mass.

PACS numbers: 12.60.-i, 12.60.Cn, 14.70.Fm, 29.20.Ej

I. INTRODUCTION

The W^\pm boson pair production process

$$e^+ + e^- \rightarrow W^+ + W^- \quad (1)$$

is a crucial one for studying the electroweak gauge symmetry in e^+e^- annihilation. Properties of the weak gauge bosons are closely related to electroweak symmetry breaking and the structure of the gauge sector in general. Thus, detailed examination of (1) at the ILC will both test this sector of the standard model (SM) with the highest accuracy and throw light on New Physics (NP) that may appear beyond the SM.

In the SM, for zero electron mass, the process (1) is described by the amplitudes mediated by photon and Z boson exchange in the s -channel and by neutrino exchange in the t -channel. Therefore, this reaction is particularly sensitive to both the leptonic vertices and the trilinear couplings to W^+W^- of the SM Z and of any new heavy neutral boson that can be exchanged in the s -channel. A popular example in this regard, is represented by the Z' 's envisaged by electroweak scenarios based on spontaneously broken ‘extended’ gauge symmetries, with masses much larger than M_Z and coupling constants different from the SM. The variety of the proposed Z' models is broad. Therefore, rather than attempting an exhaustive analysis, we shall here focus on the phenomenological effects in reaction (1) of the so-called Z'_{SSM} , Z'_{E_6} and Z'_{LR} models. Actually, in some sense, we may consider these Z' models as representative of this New Physics (NP) sector [1–8].

The direct manifestation of Z' 's would be the observation of peaks in cross sections at very high energy colliders, this would be possible only for $M_{Z'}$ lying within the kinematical reach of the machine and sufficient luminosity. Indeed, current lower limits on $M_{Z'}$ are obtained from direct searches of Z' 's in Drell-Yan dilepton pair production at the CERN LHC: from the analysis of the 7 TeV data, the observed bounds at 95% C. L. range approximately in the interval 1.8 – 2.3 TeV, depending on the particular Z' model being tested [9, 10]. For too high masses, Z' exchanges can manifest themselves indirectly, *via* deviations of cross sections, and in general of the reaction observables, from the SM predictions. Clearly, this kind of searches requires great precision and therefore will be favoured by extremely high collider luminosity, such as will be available at the ILC. Indirect lower bounds on Z' masses from the high precision LEP data at the Z lie in the range $\sim 0.4 - 1.8$ TeV, depending on the model considered [7, 8].

Indirect effects may be quite subtle, as far as the identification of the source of an observed deviation is concerned, because *a priori* different NP scenarios may lead to the same or similar experimental signatures. Clearly, then, the discrimination of one NP model (in our case the Z') from other possible ones needs an appropriate strategy for analyzing the data.¹

In this paper, we study the indirect effects evidencing the mentioned extra Z' gauge bosons in W^\pm pair production (1) at the next generation e^+e^- International Linear Collider (ILC), with a center of mass energy $\sqrt{s} = 0.5\text{--}1$ TeV and typical time-integrated luminosities of $\mathcal{L}_{\text{int}} \sim 0.5 - 1 \text{ ab}^{-1}$ [12, 13]. At the foreseen, really high luminosity this process should be quite sensitive to the indirect NP effects at a collider with $M_Z \ll \sqrt{s} \ll M_{Z'}$ [14–19], the deviations of cross sections from the SM predictions being expected to increase with \sqrt{s} due to the violation of the SM gauge cancellation among the different contributions.

Along the lines of the previous discussion, apart from estimating the foreseeable sensitivity of process (1) to the considered Z' models, we will consider the problem of establishing the potential of ILC of distinguishing the Z' effects, once observed, from the ones due to NP competitor models that can lead to analogous physical signatures in the cross section. For the latter, we will choose the models with Anomalous Gauge Couplings (AGC), and compare them with the hypothesis of Z' exchanges. In the AGC models, there is no new gauge boson exchange, but the $WW\gamma$, WWZ couplings are modified with respect to the SM values, this violates the SM gauge cancellation too and leads to deviations of the process cross sections. AGC couplings are described *via* a sum of effective interactions, ordered by dimensionality, and we shall restrict our analysis to the dimension-six terms which conserve C and P [20, 21].

The baseline configuration of the ILC envisages a very high electron beam polarization (larger than 80%) that is measurable with high precision. Also positron beam polarization, around 30%, might be initially obtainable, and this polarization could be raised to about 60% or higher in the ultimate upgrade of the machine. As is well-known, the polarization option represents an asset in order to enhance the discovery reaches and identification sensitivities on NP models of any kind [22, 23]. This is the case, in particular, of Z' exchanges and AGC interactions in process (1), an obvious example being the suppression of the ν -exchange channel by using right-handed electrons. Additional ILC diagnostic ability in Z' s and AGC

¹ Actually, this should be necessary also in the case of direct discovery, because different NP models may in principle produce the same peaks at the same mass so that, for example, for model identification some angular analyses must be applied, see [11] and references therein.

would be provided by measures of polarized W^+ and W^- in combination with initial beam polarizations.

The paper is organized as follows. In Section II, we briefly review the models involving additional Z' bosons and emphasize the role of Z - Z' mixing in the process (1). In Section III we give the parametrization of Z' and AGC effects, as well as formulae for helicity amplitudes and cross sections of the process under consideration. Section IV contains, for illustrative purposes, some plots of the unpolarized and polarized cross sections showing the effect of Z' and of Z - Z' mixing. In Section V we present the approach, which allows to obtain the discovery reach on Z' parameters (actually, on the deviations of the transition amplitudes from the SM) and the obtained numerical results. Section VI includes the results of both model dependent and model independent analyses of the possibilities to differentiate Z' effects from similar ones caused by AGC. Finally we conclude in Section VII.

II. Z' MODELS AND Z - Z' MIXING

The Z' models that will be considered in our analysis are the following [1, 2, 4, 6]:

- (i) The four possible $U(1)$ Z' scenarios originating from the spontaneous breaking of the exceptional group E_6 . In this case, two extra, heavy neutral gauge bosons appear as consequence of the symmetry breaking and, generally, only the lightest is assumed to be within reach of the collider. It is defined, in terms of a new mixing angle β , by the linear combination

$$Z' = Z'_\chi \cos \beta + Z'_\psi \sin \beta. \quad (2)$$

Specific choices of β : $\beta = 0$; $\beta = \pi/2$; $\beta = -\arctan \sqrt{5/3}$ and $\beta = \arctan \sqrt{3/5}$, corresponding to different E_6 breaking patterns, define the popular scenarios Z'_χ , Z'_ψ , Z'_η and Z'_I , respectively.

- (ii) The left-right models, originating from the breaking down of an $SO(10)$ grand-unification symmetry, and where the corresponding Z'_{LR} couple to a linear combination of right-handed and $B-L$ neutral currents (B and L being baryon and lepton numbers, respectively):

$$J_{\text{LR}}^\mu = \alpha_{\text{LR}} J_{3R}^\mu - \frac{1}{2\alpha_{\text{LR}}} J_{B-L}^\mu \quad \text{with} \quad \alpha_{\text{LR}} = \sqrt{\frac{c_W^2}{s_W^2} \kappa^2 - 1}. \quad (3)$$

Here, $s_W = \sin \theta_W$, $c_W = \sqrt{1 - s_W^2}$, additional parameters are the ratio $\kappa = g_R/g_L$ of the $SU(2)_{L,R}$ gauge couplings and α_{LR} , restricted to the range $\sqrt{2/3} \lesssim \alpha_{LR} \lesssim 1.52$. The upper bound corresponds to the so-called LR-symmetric Z'_{LRS} model with $g_R = g_L$, while the lower bound is found to coincide with the Z'_χ model introduced above. We will consider the former one, Z'_{LRS} , throughout the paper.

- (iii) The Z'_{ALR} predicted by the so-called ‘alternative’ left-right scenario. For the LR model we need not introduce additional fermions to cancel anomalies. However, in the E_6 case a variant of this model (called the Alternative LR model) can be constructed by altering the embeddings of the SM and introducing exotic fermions into the ordinary 10 and 5 representations.
- (iv) The so-called sequential Z'_{SSM} , where the couplings to fermions are the same as those of the SM Z .

Detailed descriptions of these models, as well as the specific references, can be found, e. g., in Refs. [1, 2, 4, 6].

In the extended gauge theories predicting the existence of an extra neutral Z' gauge boson, the mass-squared matrix of the Z and Z' can have non-diagonal entries δM^2 , which are related to the vacuum expectation values of the fields of an extended Higgs sector [4]:

$$M_{ZZ'}^2 = \begin{pmatrix} M_Z^2 & \delta M^2 \\ \delta M^2 & M_{Z'}^2 \end{pmatrix}. \quad (4)$$

Here, Z and Z' denote the weak gauge boson eigenstates of $SU(2)_L \times U(1)_Y$ and of the extra $U(1)'$, respectively. The mass eigenstates, Z_1 and Z_2 , diagonalizing the matrix (4), are then obtained by the rotation of the fields Z and Z' by a mixing angle ϕ :

$$Z_1 = Z \cos \phi + Z' \sin \phi, \quad (5)$$

$$Z_2 = -Z \sin \phi + Z' \cos \phi. \quad (6)$$

Here, the mixing angle ϕ is expressed in terms of masses as:

$$\tan^2 \phi = \frac{M_Z^2 - M_1^2}{M_2^2 - M_Z^2} \simeq \frac{2M_Z \Delta M}{M_2^2}, \quad (7)$$

where $\Delta M = M_Z - M_1 > 0$, M_Z is the mass of the Z_1 -boson in the absence of mixing, i.e., for $\phi = 0$. Once we assume the mass M_1 to be determined experimentally, the mixing

depends on two free parameters, which we identify as ϕ and M_2 . We shall here consider the configuration $M_1 \ll \sqrt{s} \ll M_2$.

The mixing angle ϕ will play an important role in our analysis. In general, such mixing effects reflect the underlying gauge symmetry and/or the Higgs sector of the model. To a good approximation, for $M_1 \ll M_2$, in specific “minimal-Higgs models” [24],

$$\phi \simeq -s_W^2 \frac{\sum_i \langle \Phi_i \rangle^2 I_{3L}^i Q'_i}{\sum_i \langle \Phi_i \rangle^2 (I_{3L}^i)^2} = \mathcal{C} \frac{M_1^2}{M_2^2}. \quad (8)$$

Here $\langle \Phi_i \rangle$ are the Higgs vacuum expectation values spontaneously breaking the symmetry, and Q'_i are their charges with respect to the additional $U(1)'$. In addition, in these models the same Higgs multiplets are responsible for both generation of mass M_1 and for the strength of the Z - Z' mixing [1]. Thus \mathcal{C} is a model-dependent constant. For example, in the case of E_6 superstring-inspired models \mathcal{C} can be expressed as [24]

$$\mathcal{C} = 4s_W \left(A - \frac{\sigma - 1}{\sigma + 1} B \right), \quad (9)$$

where σ is the ratio of vacuum expectation values squared, and the constants A and B are determined by the mixing angle β : $A = \cos \beta / 2\sqrt{6}$, $B = \sqrt{10}/12 \sin \beta$.

An important property of the models under consideration is that the gauge eigenstate Z' does not couple to the W^+W^- pair since it is neutral under $SU(2)_L$. Therefore the process (1), and the searched-for deviations of the cross sections from the SM, are sensitive to a Z' only in the case of a non-zero Z - Z' mixing. The mixing angle is rather highly constrained, to an upper limit of a few $\times 10^{-3}$, mainly from LEP measurements at the Z [7, 8]. The high statistics on W -pair production expected at the ILC might in principle allow to probe such small mixing angles effectively.

From (5) and (6), one obtains the vector and axial-vector couplings of the Z_1 and Z_2 bosons to fermions:

$$v_{1f} = v_f \cos \phi + v'_f \sin \phi, \quad a_{1f} = a_f \cos \phi + a'_f \sin \phi, \quad (10)$$

$$v_{2f} = -v_f \sin \phi + v'_f \cos \phi, \quad a_{2f} = -a_f \sin \phi + a'_f \cos \phi, \quad (11)$$

with $(v_f, a_f) = (g_L^f \pm g_R^f)/2$, and (v'_f, a'_f) similarly defined in terms of the Z' couplings. The fermionic Z' couplings can be found in [1, 2, 4, 6].

Analogously, one obtains according to the remarks above:

$$g_{WWZ_1} = \cos \phi g_{WWZ}, \quad (12)$$

$$g_{WWZ_2} = -\sin \phi g_{WWZ}, \quad (13)$$

where $g_{WWZ} = \cot \theta_W$.

III. PARAMETERIZATIONS OF Z' -BOSON AND AGC EFFECTS

A. Z' boson

The starting point of our analysis will be the amplitude for the process (1). In the Born approximation, this can be written as a sum of a t -channel and an s -channel component. In the SM case, the latter will be schematically written as follows:

$$\mathcal{M}_s^{(\lambda)} = \left(-\frac{1}{s} + \frac{\cot \theta_W (v - 2\lambda a)}{s - M_Z^2} \right) \times \mathcal{G}^{(\lambda)}(s, \theta), \quad (14)$$

where s and θ are the total c.m. squared energy and W^- production angle. Omitting the fermion subscripts, electron vector and axial-vector couplings in the SM are denoted as $v = (T_{3,e} - 2Q_e s_W^2)/2s_W c_W$ and $a = T_{3,e}/2s_W c_W$, respectively, with $T_{3,e} = -1/2$, and λ denoting the electron helicity ($\lambda = \pm 1/2$ for right/left-handed electrons). Finally, $\mathcal{G}^{(\lambda)}(s, \theta)$ is a kinematical coefficient, depending also on the W^\pm helicities. The explicit form can be found in the literature [20, 21] or derived from the entries of Table V, which also shows the form of the t -channel neutrino exchange.

In the extended gauge models the process (1) is described by the set of diagrams displayed in Fig. 1. The amplitude with the extra Z' depicted in Fig. 1 will be written as:

$$\mathcal{M}_s^{(\lambda)} = \left(-\frac{1}{s} + \frac{g_{WWZ_1}(v_1 - 2\lambda a_1)}{s - M_1^2} + \frac{g_{WWZ_2}(v_2 - 2\lambda a_2)}{s - M_2^2} \right) \times \mathcal{G}^{(\lambda)}(s, \theta). \quad (15)$$

The contribution of the new heavy neutral gauge boson Z_2 to the amplitude of process (1) is represented by the fourth diagram in Fig. 1. In addition, there are indirect contributions to the Z_1 -mediated diagram, represented by modifications of the electron and three-boson vertices induced by the Z - Z' mixing.

It is convenient to rewrite Eq. (15) in the following form [17]:²

$$\mathcal{M}_s^{(\lambda)} = \left(-\frac{g_{WW\gamma}}{s} + \frac{g_{WWZ}(v - 2\lambda a)}{s - M_Z^2} \right) \times \mathcal{G}^{(\lambda)}(s, \theta), \quad (16)$$

where the ‘effective’ gauge boson couplings $g_{WW\gamma}$ and g_{WWZ} are defined as:

$$g_{WW\gamma} = 1 + \Delta_\gamma = 1 + \Delta_\gamma(Z_1) + \Delta_\gamma(Z_2), \quad (17)$$

² Note that $M_Z = M_1 + \Delta M$, where M_1 refers to the mass eigenstate.

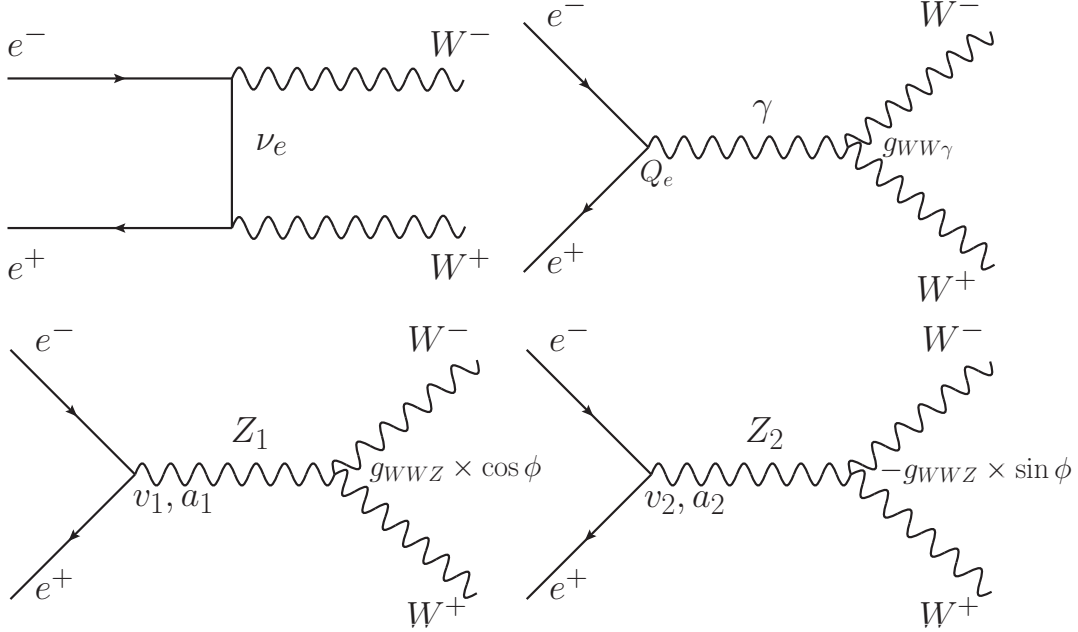


FIG. 1: Feynman diagrams for the process $e^-e^+ \rightarrow W^-W^+$ in the Born approximation

$$g_{WWZ} = \cot \theta_W + \Delta_Z = \cot \theta_W + \Delta_Z(Z_1) + \Delta_Z(Z_2), \quad (18)$$

with

$$\Delta_\gamma(Z_1) = v \cot \theta_W \left(\frac{\Delta a}{a} - \frac{\Delta v}{v} \right) (1 + \Delta\chi) \chi; \quad \Delta_\gamma(Z_2) = v g_{WWZ_2} \left(\frac{a_2}{a} - \frac{v_2}{v} \right) \chi_2, \quad (19)$$

$$\Delta_Z(Z_1) = \Delta g_{WWZ} + \cot \theta_W \left(\frac{\Delta a}{a} + \Delta\chi \right); \quad \Delta_Z(Z_2) = g_{WWZ_2} \frac{a_2}{a} \frac{\chi_2}{\chi}. \quad (20)$$

In Eqs. (19) and (20) we have introduced the deviations of the fermionic and trilinear bosonic couplings $\Delta v = v_1 - v$, $\Delta a = a_1 - a$ and $\Delta g_{WWZ} = g_{WWZ_1} - \cot \theta_W$, and the neutral vector boson propagators (neglecting their widths):

$$\chi(s) = \frac{s}{s - M_Z^2}; \quad \chi_2(s) = \frac{s}{s - M_2^2}; \quad \Delta\chi(s) \simeq -\frac{2M_Z\Delta M}{s - M_Z^2}, \quad (21)$$

where $\Delta M = M_Z - M_1$ is the Z - Z_1 mass shift. Because W pair production is studied sufficiently far away from the Z_1 peak, we can neglect the Z and $Z_{1,2}$ widths in (15) and (16).

It should be stressed that, not referring to specific models, the parametrization (16)-(18) is both general and useful for phenomenological purposes, in particular to compare different sources of nonstandard effects contributing finite deviations (19) and (20) to the SM predictions. Note that Δ_γ vanishes as $s \rightarrow 0$, consistent with gauge invariance.

We know from current measurements [7] that $\Delta M < 100$ MeV. This allows the approximation $\Delta\chi(s) \ll 1$. One can rewrite (19) and (20) in a simplified form taking into account the approximation above as well as the couplings to first order in ϕ as:

$$(v_1, a_1) \simeq (v + v'\phi, a + a'\phi) \Rightarrow (\Delta v, \Delta a) \simeq (v'\phi, a'\phi), \quad (22)$$

$$(v_2, a_2) \simeq (-v\phi + v', -a\phi + a'), \quad (23)$$

and

$$g_{WWZ_1} \simeq g_{WWZ}; \quad g_{WWZ_2} \simeq -g_{WWZ}\phi. \quad (24)$$

In the case of extended models considered here, e.g. E_6 , v' and a' are explicitly parametrized in terms of the angle β which characterizes the direction of the Z' -related extra $U(1)'$ generator in the E_6 group space, and reflects the pattern of symmetry breaking to $SU(2)_L \times U(1)_Y$ [1, 2, 4, 6]:

$$v' = \frac{\cos\beta}{c_W\sqrt{6}}; \quad a' = \frac{1}{2c_W\sqrt{6}} \left(\cos\beta + \sqrt{\frac{5}{3}} \sin\beta \right). \quad (25)$$

Substituting Eqs. (22)–(24) into (19) and (20), one finds the general form of Δ_γ and Δ_Z :

$$\Delta_\gamma = \phi \cdot v \cot\theta_W \left(\frac{a'}{a} - \frac{v'}{v} \right) \left(1 - \frac{\chi_2}{\chi} \right) \chi, \quad (26)$$

$$\Delta_Z = \phi \cdot \cot\theta_W \frac{a'}{a} \left(1 - \frac{\chi_2}{\chi} \right). \quad (27)$$

Both these quantities have the *same* dependence on ϕ and M_2 , via the product $\phi(1 - \chi_2/\chi)$. Thus, ϕ and M_2 can not be separately determined from a measurement of Δ_γ and Δ_Z , only this composite function can be determined. We also note that for an SSM-type model, the first parenthesis in Eq. (26) vanishes, resulting in $\Delta_\gamma = 0$. Thus, these models can not be distinguished from the AGC models, introduced in the next section. Further, the terms proportional to χ_2 in Eqs. (26) and (27) dominate in the case $\sqrt{s} \approx M_2$ but will be very small in the case $\sqrt{s} \ll M_2$.

B. Anomalous Gauge Couplings

As pointed out in the Introduction, a model with an extra Z' would produce virtual manifestations in the final W^+W^- channel at the ILC that in principle could mimic those of a model with AGC, hence of completely different origin. This is due to the fact that, as

shown above, the effects of the extra Z' can be reabsorbed into a redefinition of the WWV couplings ($V = \gamma, Z$). Therefore, the identification of such an effect, if observed at the ILC, becomes a very important problem [25].

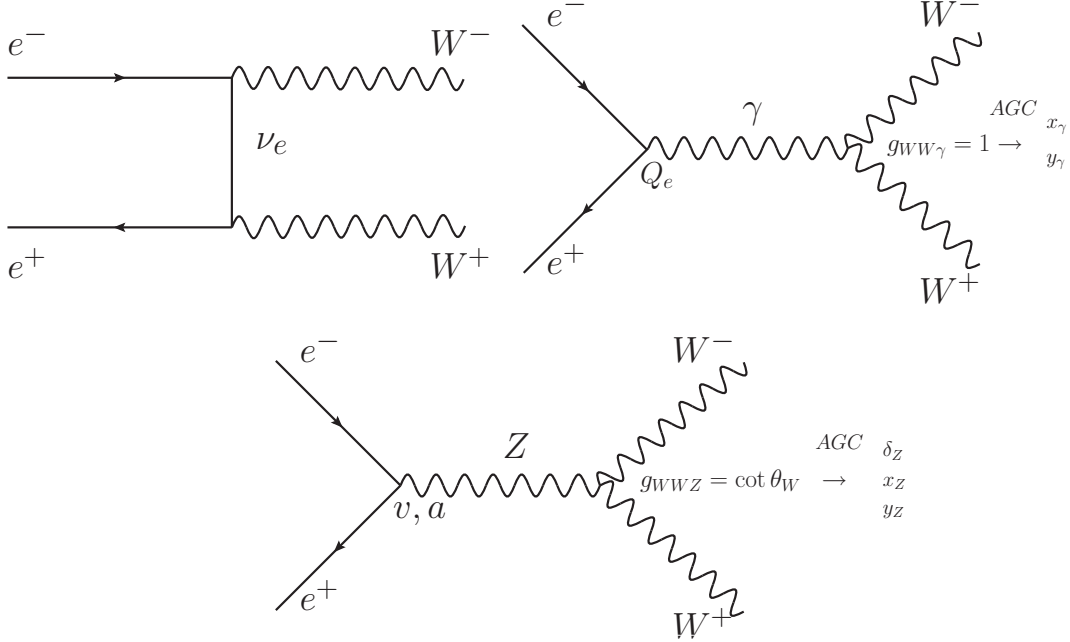


FIG. 2: Feynman diagrams for the process $e^+e^- \rightarrow W^+W^-$ in the Standard Model and with anomalous trilinear gauge couplings (AGC).

Using the notations of, e.g., Ref. [20, 21], the relevant trilinear WWV interaction up to operators of dimension-6, which conserves $U(1)_{\text{e.m.}}$, C and P , can be written as ($e = \sqrt{4\pi\alpha_{em}}$):

$$\begin{aligned}
\mathcal{L}_{\text{eff}} = & -ie [A_\mu (W^{-\mu\nu}W_\nu^+ - W^{+\mu\nu}W_\nu^-) + F_{\mu\nu}W^{+\mu}W^{-\nu}] \\
& - ie (\cot \theta_W + \delta_Z) [Z_\mu (W^{-\mu\nu}W_\nu^+ - W^{+\mu\nu}W_\nu^-) + Z_{\mu\nu}W^{+\mu}W^{-\nu}] \\
& - ie x_\gamma F_{\mu\nu}W^{+\mu}W^{-\nu} - ie x_Z Z_{\mu\nu}W^{+\mu}W^{-\nu} \\
& + ie \frac{y_\gamma}{M_W^2} F^{\nu\lambda}W_{\lambda\mu}^-W_\nu^{+\mu} + ie \frac{y_Z}{M_W^2} Z^{\nu\lambda}W_{\lambda\mu}^-W_\nu^{+\mu}, \tag{28}
\end{aligned}$$

where $W_{\mu\nu}^\pm = \partial_\mu W_\nu^\pm - \partial_\nu W_\mu^\pm$ and $Z_{\mu\nu} = \partial_\mu Z_\nu - \partial_\nu Z_\mu$. In the SM at the tree-level, the anomalous couplings in (28) vanish: $\delta_Z = x_\gamma = x_Z = y_\gamma = y_Z = 0$.

The anomalous gauge couplings are here parametrized in terms of five real independent parameters. This number can be reduced by imposing additional constraints, like local

$SU(2)_L \times U(1)_Y$ symmetry, in which case the number would be reduced to three (see for example Tables 2 and 1 of [26] and [27], respectively).

Current limits reported by the Particle Data Group [28], that show the sensitivity to the AGCs attained so far, are roughly of the order of 0.04 for δ_Z , 0.05 for x_γ , 0.02 for y_γ , 0.11 for x_Z and 0.12 for y_Z . As will be shown in the next sections, at the ILC in the energy and luminosity configuration considered here, sensitivities to deviations from the SM, hence of indirect New Physics signatures, down to the order of 10^{-3} will be reached. This would compare with the expected order of magnitude of the theoretical uncertainty on the SM cross sections after accounting for higher-order corrections to the Born amplitudes of Figs. 1 and 2, formally of order α_{em} [29, 30], but that for distributions can reach the size of 10%, depending on \sqrt{s} [31, 32].

C. Helicity amplitudes and cross sections

The general expression for the cross section of process (1) with longitudinally polarized electron and positron beams described by the set of diagrams presented in Fig. 2 can be expressed as

$$\frac{d\sigma}{d\cos\theta} = \frac{1}{4} \left[(1 + P_L) (1 - \bar{P}_L) \frac{d\sigma^+}{d\cos\theta} + (1 - P_L) (1 + \bar{P}_L) \frac{d\sigma^-}{d\cos\theta} \right], \quad (29)$$

where P_L and \bar{P}_L are the actual degrees of electron and positron longitudinal polarization, respectively, and σ^\pm are the cross sections for purely right-handed ($\lambda = 1/2$) and left-handed ($\lambda = -1/2$) electrons. From Eq. (29), the cross section for polarized (unpolarized) electrons and unpolarized positrons corresponds to $P_L \neq 0$ and $\bar{P}_L = 0$ ($P_L = \bar{P}_L = 0$).

The polarized cross sections can generally be written as follows:

$$\frac{d\sigma^\pm}{d\cos\theta} = \frac{|\mathbf{p}|}{16\pi s\sqrt{s}} \sum_{\tau,\tau'} |F_{\lambda\tau\tau'}(s, \cos\theta)|^2. \quad (30)$$

Here, the helicities of the W^- and W^+ are denoted by $\tau, \tau' = \pm 1, 0$. Corresponding to the interaction (28), the helicity amplitudes $F_{\lambda\tau\tau'}(s, \cos\theta)$ have the structure shown in Table V [20, 21] in Appendix A. In Table V, $\beta_W = \sqrt{1 - 4M_W^2/s} = 2p/\sqrt{s}$, with $p = |\mathbf{p}|$ the c.m. momentum of the W^- . Furthermore, s and t are the Mandelstam variables, and θ the c.m. scattering angle, with $t = M_W^2 - s(1 - \beta \cos\theta)/2$. For comparison, we also show in Appendix A the corresponding helicity amplitudes for the case of a Z' .

We define the differential cross sections for correlated spins of the produced W^- and W^+ ,

$$\frac{d\sigma(W_L^+W_L^-)}{d\cos\theta}, \quad \frac{d\sigma(W_T^+W_T^-)}{d\cos\theta}, \quad \frac{d\sigma(W_T^+W_L^- + W_L^+W_T^-)}{d\cos\theta}, \quad (31)$$

which correspond to the production of two longitudinally ($\tau = \tau' = 0$), two transversely ($\tau = \pm\tau'$; $\tau, \tau' = \pm 1$) and one longitudinally plus one transversely ($\tau = 0, \tau' = \pm 1$ etc.) polarized vector bosons, respectively.

IV. Z' ILLUSTRATIONS

For illustrative purposes, the energy behavior of the total unpolarized cross section for the process $e^+e^- \rightarrow W^+W^-$ is shown in Fig. 3 (top panel) for the SM (extrapolated to 2 TeV) as well as for the case of an additional Z'_χ originated from E_6 at mixing angle $\phi = \pm 1.6 \cdot 10^{-3}$ and $M_{Z'} = 2$ TeV. In the lower panel we show the corresponding cross section for right-handed electrons ($P_L = 1$). The deviation of the cross sections from the SM prediction caused by the Z' boson at the planned ILC energy of $\sqrt{s} = 0.5$ TeV is most pronounced for the latter (polarized) case while the cross section is lower than that for unpolarized beams. The main reason for this is the removal of the neutrino exchange in the t -channel. Such a removal is indispensable for evidencing the Z' -exchange effect through Z - Z' mixing in the process (1). The complete removal of the neutrino exchange contribution depends of course on having pure electron polarization. In both cases experimental constraints on the W^- scattering angle ($|\cos\theta| \leq 0.98$) were imposed.

The effects of the Z' boson shown in Fig. 3 were parametrized by the mass $M_{Z'}$ and the Z - Z' mixing angle ϕ while those behaviors and their relative deviations shown in Fig. 4, are parametrized by the effective parameters $(\Delta_\gamma, \Delta_Z)$, defined in Eqs. (26) and (27) for the same values of ϕ and $M_{Z'}$. Rather steep energy behavior of relative deviations of the cross sections can be appreciated from Fig. 4.

As was mentioned in the Introduction, the process (1) is sensitive to a Z' in the case of non-zero Z - Z' mixing. The individual (interference) contributions to the cross section of process (1) rise proportional to s . In the SM, the sum over all contributions to the total cross section results in its proper energy dependence that scales like $\log s/s$ in the limit when $2M_W \ll \sqrt{s} \ll M_2$ due to a delicate gauge cancellation. In the case of a non-zero Z - Z' mixing, the couplings of the Z_1 differ from those of the SM predictions for Z . Then,

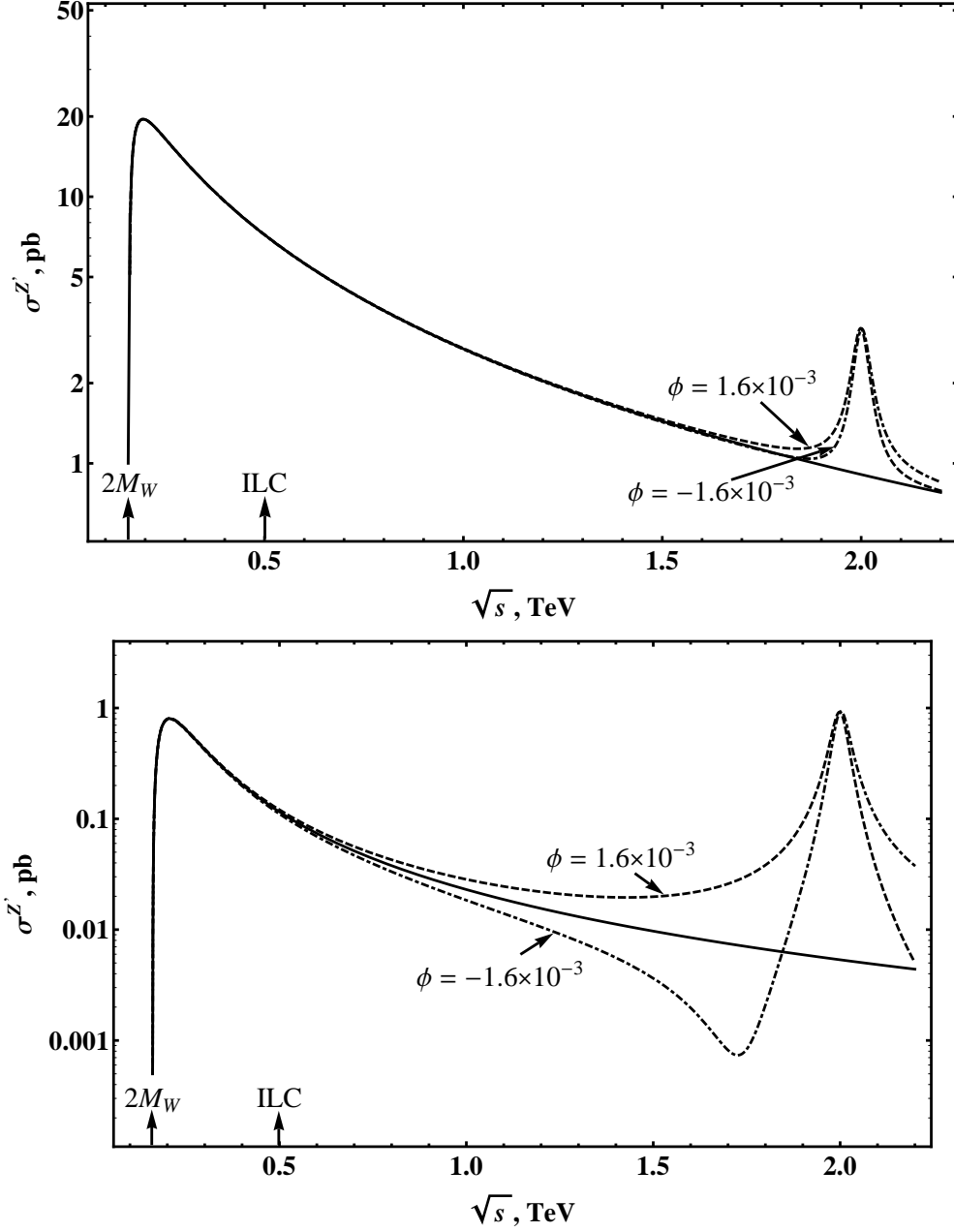


FIG. 3: Top panel: Unpolarized total cross section for the process $e^+e^- \rightarrow W^+W^-$ for Z'_χ from E_6 . Bottom panel: Polarized total cross section. Solid lines correspond to the SM case. Dashed (dash-dotted) lines correspond to a Z' model with $\phi = 1.6 \cdot 10^{-3}$ ($\phi = -1.6 \cdot 10^{-3}$), $\Gamma_2 = 0.025 \times M_2$ and $M_2 = 2$ TeV.

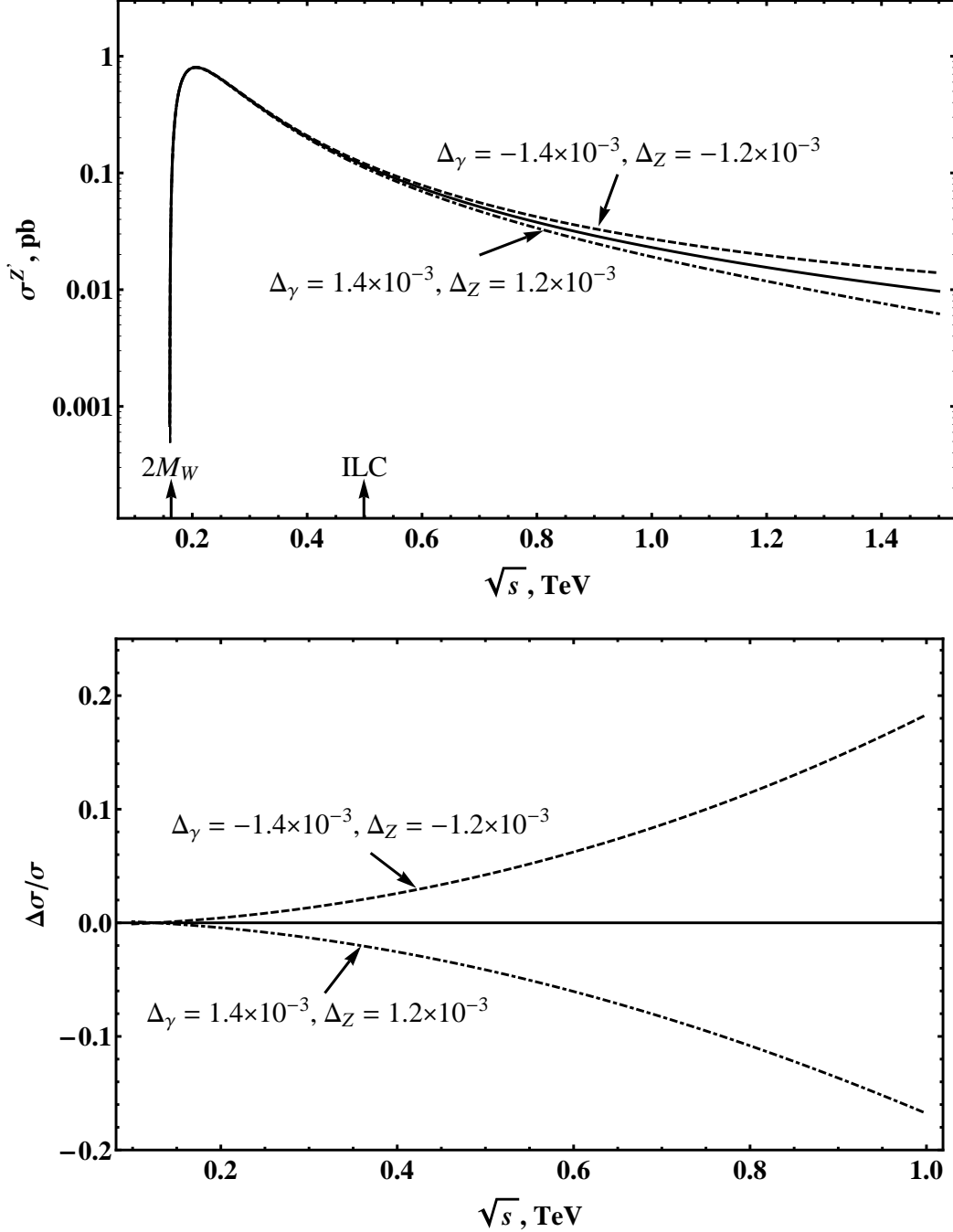


FIG. 4: Top panel: Polarized total cross section for the process $e^+e^- \rightarrow W^+W^-$ as a function of \sqrt{s} with perfectly polarized electrons ($P_L = 1$) and unpolarized final states. Solid line corresponds to the SM. Contribution to the cross section caused by Z' is determined by different sets of parameters $(\Delta_\gamma, \Delta_Z) = (1.4 \cdot 10^{-3}, 1.2 \cdot 10^{-3})$ and $(-1.4 \cdot 10^{-3}, -1.2 \cdot 10^{-3})$. Bottom panel: Relative deviation of the polarized total cross section from the SM prediction, $\Delta\sigma/\sigma = (\sigma^{Z'} - \sigma^{SM})/\sigma^{SM}$.

the gauge cancellation occurring in the SM is destroyed, leading to an enhancement of new physics effects at high energies, though well below M_2 . Unitarity is restored only at energies $\sqrt{s} \gg M_2$ independently of details of the extended gauge group.

V. DISCOVERY REACH ON Z' PARAMETERS

The sensitivity of the polarized differential cross sections to Δ_γ and Δ_Z is assessed numerically by dividing the angular range $|\cos\theta| \leq 0.98$ into 10 equal bins, and defining a χ^2 function in terms of the expected number of events $N(i)$ in each bin for a given combination of beam polarizations:

$$\chi^2 = \chi^2(\sqrt{s}, \Delta_\gamma, \Delta_Z) = \sum_{\{P_L, \bar{P}_L\}} \sum_i^{\text{bins}} \left[\frac{N_{\text{SM}+Z'}(i) - N_{\text{SM}}(i)}{\delta N_{\text{SM}}(i)} \right]^2, \quad (32)$$

where $N(i) = \mathcal{L}_{\text{int}} \sigma_i \varepsilon_W$ with \mathcal{L}_{int} the time-integrated luminosity. Furthermore,

$$\sigma_i = \sigma(z_i, z_{i+1}) = \int_{z_i}^{z_{i+1}} \left(\frac{d\sigma}{dz} \right) dz, \quad (33)$$

where $z = \cos\theta$ and polarization indices have been suppressed. Also, ε_W is the efficiency for W^+W^- reconstruction, for which we take the channel of lepton pairs ($e\nu + \mu\nu$) plus two hadronic jets, giving $\varepsilon_W \simeq 0.3$ basically from the relevant branching ratios. The procedure outlined above is followed to evaluate both $N_{\text{SM}}(i)$ and $N_{\text{SM}+Z'}(i)$.

The uncertainty on the number of events $\delta N_{\text{SM}}(i)$ combines both statistical and systematic errors where the statistical component is determined by $\delta N_{\text{SM}}^{\text{stat}}(i) = \sqrt{N_{\text{SM}}(i)}$. Concerning systematic uncertainties, an important source is represented by the uncertainty on beam polarizations, for which we assume $\delta P_L/P_L = \delta \bar{P}_L/\bar{P}_L = 0.5\%$ with the ‘‘standard’’ envisaged values $|P_L| = 0.8$ and $|\bar{P}_L| = 0.5$ [12, 13, 22]. As for the time-integrated luminosity, for simplicity we assume it to be equally distributed between the different polarization configurations. Another source of systematic uncertainty originates from the efficiency of reconstruction of W^\pm pairs which we assume to be $\delta\varepsilon_W/\varepsilon_W = 0.5\%$. Also, in our numerical analysis to evaluate the sensitivity of the differential distribution to model parameters we include initial-state QED corrections to on-shell W^\pm pair production in the flux function approach [33, 34] that assures a good approximation within the expected accuracy of the data.

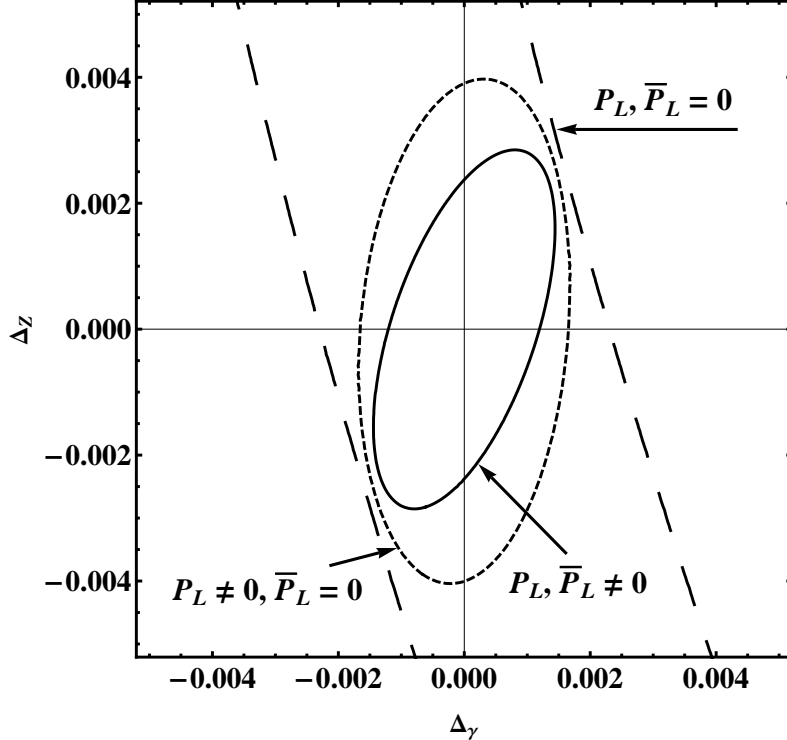


FIG. 5: Discovery reach (see Eq. (34)) at 95% CL on the Z' parameters Δ_γ, Δ_Z obtained from polarized differential cross sections at different sets of polarization: $P_L = \pm 0.8, \bar{P}_L = \mp 0.5$ (solid line), $P_L = \pm 0.8, \bar{P}_L = 0$ (short-dashed line), unpolarized beams $P_L = 0, \bar{P}_L = 0$ (long-dashed line), $\sqrt{s} = 0.5$ TeV and $\mathcal{L}_{\text{int}} = 500 \text{ fb}^{-1}$.

As a criterion to derive the constraints on the coupling constants in the case where no deviations from the SM were observed within the foreseeable uncertainties on the measurable cross sections, we impose that

$$\chi^2 \leq \chi_{\text{min}}^2 + \chi_{\text{CL}}^2, \quad (34)$$

where χ_{CL}^2 is a number that specifies the chosen confidence level, χ_{min}^2 is the minimal value of the χ^2 function. With two independent parameters in Eqs. (17) and (18), the 95% CL is obtained by choosing $\chi_{\text{CL}}^2 = 5.99$.

From the numerical procedure outlined above, we obtain the allowed regions in Δ_γ and Δ_Z determined from the differential polarized cross sections with different sets of polarization (as well as from the unpolarized process (1)) depicted in Fig. 5, where $\mathcal{L}_{\text{int}} = 500 \text{ fb}^{-1}$ has been taken [12, 13, 22]. According to the condition (34), the values of Δ_γ and Δ_Z for which Z' s can be discovered at the ILC is represented by the region external to the ellipse. The same is true for the AGC model except that, having assumed no renormalization of the

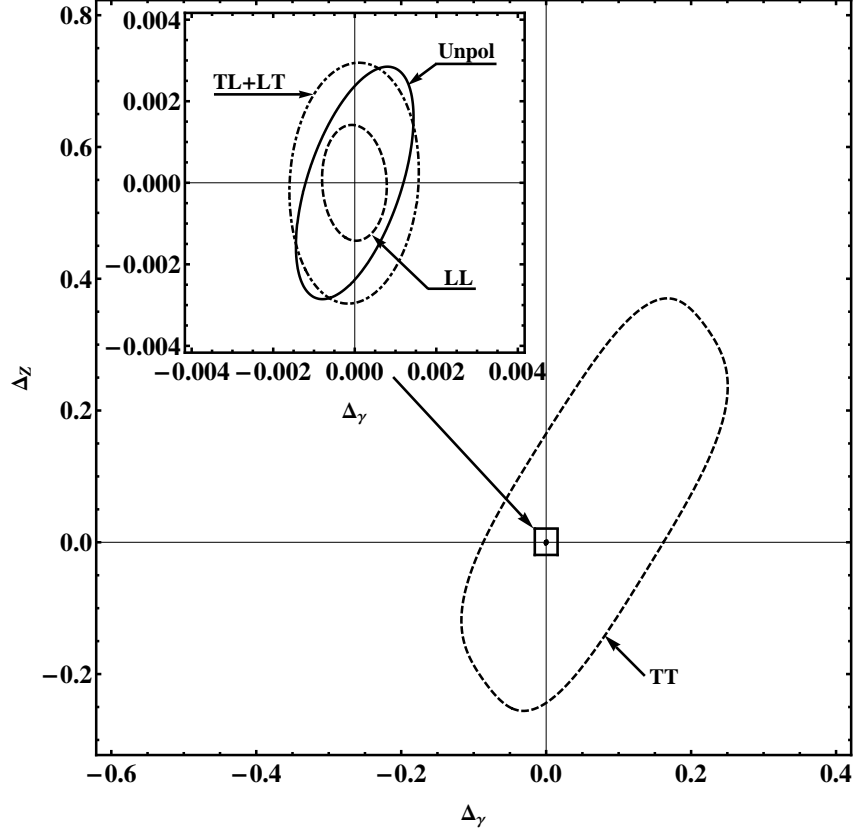


FIG. 6: Discovery reach on the Z' parameters Δ_γ, Δ_Z from the cross section with polarized beams $P_L = \pm 0.8$, $\bar{P}_L = \mp 0.5$ and different sets of W^\pm polarizations. Here, $\sqrt{s} = 0.5$ TeV and $\mathcal{L}_{\text{int}} = 500 \text{ fb}^{-1}$.

residue of the photon pole exchange ($\delta_\gamma = 0$), in this case Δ_γ will be proportional to s times the coefficients x_γ or y_γ of Eq. (28), and Δ_Z to a combination of the coefficients δ_Z, x_Z and y_Z (see Table V). The role of initial beam polarization is seen to be essential in order to set meaningful finite bounds on the parameters.

Analogous to Fig. 5, the discovery reach on the parameters Δ_γ, Δ_Z from the cross section with polarized beams $P_L = \pm 0.8$, $\bar{P}_L = \mp 0.5$ and different sets of W^\pm polarizations is depicted in Fig. 6 which demonstrates that $d\sigma(W_L^+W_L^-)/dz$ is most sensitive to the parameters Δ_γ, Δ_Z while $d\sigma(W_T^+W_T^-)/dz$ has the lowest sensitivity to those parameters. The reason for the lower sensitivity in the TT case is that for $s \gg M_Z^2$, the NP contributions to these amplitudes only interfere with a sub-dominant part of the SM amplitude [26].

As regards the NP scenarios of interest here, one may remark that constraints on Δ_γ and Δ_Z of Eqs. (17) and (18) (for the example of Z' s), are model-independent in the sense that

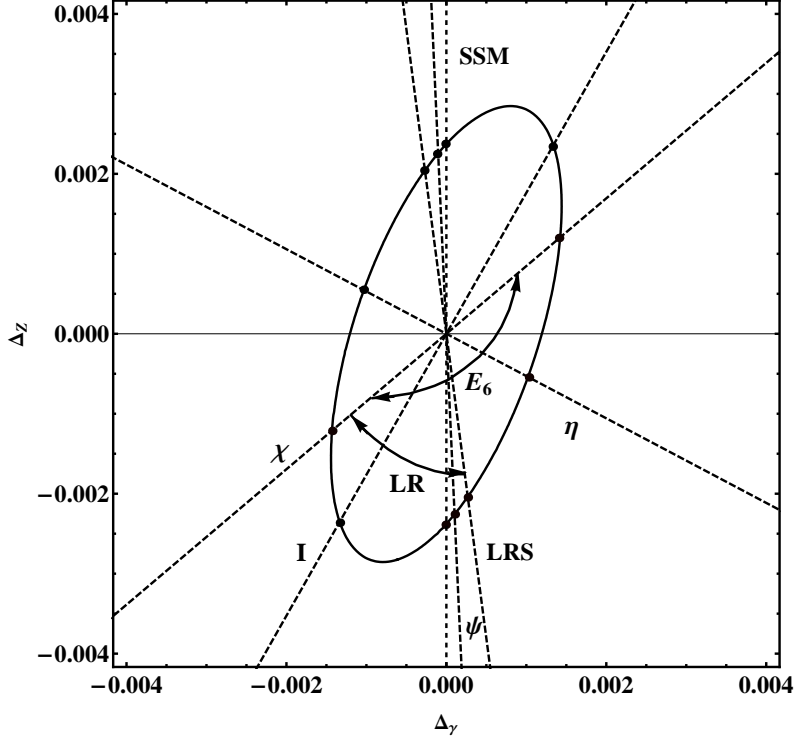


FIG. 7: Discovery reach (95% C.L.) on Z' parameters (Δ_γ , Δ_Z) obtained from differential polarized cross sections with ($P_L = \pm 0.8$, $\bar{P}_L = \mp 0.5$). Dashed straight lines correspond to specific extended gauge models (χ , ψ , η , I and LRS) according to Eq. (35). The segments of the ellipse correspond to the whole classes of E_6 and LR-models, respectively. Here, $\sqrt{s} = 0.5$ TeV and $\mathcal{L}_{\text{int}} = 500$ fb $^{-1}$.

they constrain the whole class of Z' models considered. They may turn into constraints on the parameters of specific Z' models by replacing expressions (19) and (20). Specializing to those models, one can notice the important linear relation characterizing the deviations from the SM:

$$\Delta_Z = \Delta_\gamma \cdot \frac{1}{v\chi} \frac{(a'/a)}{(a'/a) - (v'/v)}, \quad (35)$$

where v and a refer to vector and axial-vector couplings. This relation is rather unique, and depends neither on ϕ nor on M_2 , only on ratios of the electron couplings with the Z and Z' bosons.

In Fig. 7 we depict, as an illustration, the cases corresponding to the models denoted χ , ψ , η and I originated from E_6 as well as the LR symmetric model (LRS). The model independent bound on Δ_γ and Δ_Z can be converted into limits on the Z - Z' mixing angle ϕ and mass M_2 for any specific Z' model. These model dependent constraints will be presented

in the next section along with identification reaches. For fixed ϕ and M_2 , every model is represented by a point in the $(\Delta_\gamma, \Delta_Z)$ parameter plane. The discovery regions in the Δ_γ - Δ_Z plot at the ILC are represented by the straight segments lying outside the ellipse. If one varies the mixing angle ϕ , the point representative of the specific Z' model moves along the corresponding line. The intercept of the lines with the elliptic contour, once translated to ϕ and M_2 , determine the constraint on these two parameters relevant to Z - Z' mixing for the individual models.

Also, one can determine the region in the $(\Delta_\gamma, \Delta_Z)$ plane relevant to constraining the full class of E_6 (and LR) Z' models obtained by varying the parameters $\cos\beta$ and α_{LR} of Eqs. (2) and (3) within their full allowed ranges. The corresponding discovery region at the ILC for that class of models is the one delimited by the arcs of ellipse indicated in Fig. 7.

VI. IDENTIFICATION OF Z' VS AGC

A. Model independent analysis

We will here discuss how one can differentiate various Z' models from similar effects caused by anomalous gauge couplings, following the procedure employed in Refs. [23, 35]. The philosophy is as follows: A particular Z' model will be considered identified, if the measured values of Δ_γ and Δ_Z are statistically different from values corresponding to other Z' models (for a discussion, see Ref. [23]), and also different from ranges of $(\Delta_\gamma, \Delta_Z)$ that can be populated by AGC models. Clearly, at least one of these parameters must exceed some minimal value.

Let us assume the data to be consistent with one of the Z' models and call it the “true” model. It has some non-zero values of the parameters Δ_γ, Δ_Z . We want to assess the level at which this “true” model is distinguishable from the AGC models, that can compete with it as sources of the assumed deviations of the cross section from the SM and we call them “tested” models, for any values of the corresponding AGC parameters. We assume for simplicity that all AGC parameters are zero, except the one whose values are probed.

We start by considering as a “tested” AGC model that with a value of x_γ to be scanned over. To that purpose, we can define a “distance” between the chosen “true” model and the

“tested” AGC model(s) by means of a χ^2 function analogous to Eq. (32) as

$$\chi^2 = \sum_{\{P_L, \bar{P}_L\}} \sum_i^{\text{bins}} \left[\frac{N_{Z'}(i) - N_{\text{AGC}}(i)}{\delta N_{Z'}(i)} \right]^2, \quad (36)$$

with $\delta N_{Z'}(i)$ defined in the same way as $\delta N_{\text{SM}}(i)$ but, in this case, the statistical uncertainty refers to the Z' model and therefore depends on the relevant, particular, values of Δ_γ and Δ_Z .

On the basis of such χ^2 we can study whether these “tested” models can be excluded or not to a given confidence level (which we assume to be 95%), once the considered Z' model (defined in terms of Δ_γ , Δ_Z) has been assumed as “true”. In our explicit example, we want to determine the range in x_γ for which there is “confusion” of deviations from the SM cross sections between the selected “true” Z' model and the AGC one, by imposing the condition, similar to Eq. (34). Then we scan all values of Δ_γ , Δ_Z allowed by the Z' models down to their discovery reach, and determine by iteration in this procedure the general confusion region between the class of Z' models considered here and the AGC model with $x_\gamma \neq 0$.

Besides the dependence on the c.m. energy \sqrt{s} , the χ^2 function defined above can be considered a function of three independent variables, Δ_γ and Δ_Z from the Z' model, and, in our starting example, the parameter x_γ of the AGC scenario. The contours of the confusion regions, at given \sqrt{s} , are thus defined by the region *inside* of which (in the Δ_γ - Δ_Z space)

$$\chi^2(\Delta_\gamma, \Delta_Z, x_\gamma) = \chi_{\text{min}}^2 + \chi_{\text{CL}}^2, \quad (37)$$

for any value of x_γ compatible with experimental limits.

In Fig. 8 we show the region of confusion in the Z' parameter plane (Δ_γ, Δ_Z), outside of which the Z' model can be identified at the 95% C.L. against the AGC model for any value of the parameter x_γ . It is obtained from the polarized cross section with $P_L = \pm 0.8$ and $\bar{P}_L = \mp 0.5$ using the algorithm outlined above. Also, note that the inner dash-dotted ellipse in Fig. 8 delimits the discovery reach on Z' parameters.

The graphical representation of the region of confusion presented in Fig. 8 is straightforward. Equation (37) defines a three-dimensional surface enclosing a volume in the ($\Delta_\gamma, \Delta_Z, x_\gamma$) parameter space in which there can be discovery as well as confusion between Z' and (in this case) the x_γ -AGC model. The planar surface delimited by the solid ellipse is determined by the projection of such three-dimensional surface, hence of the corresponding

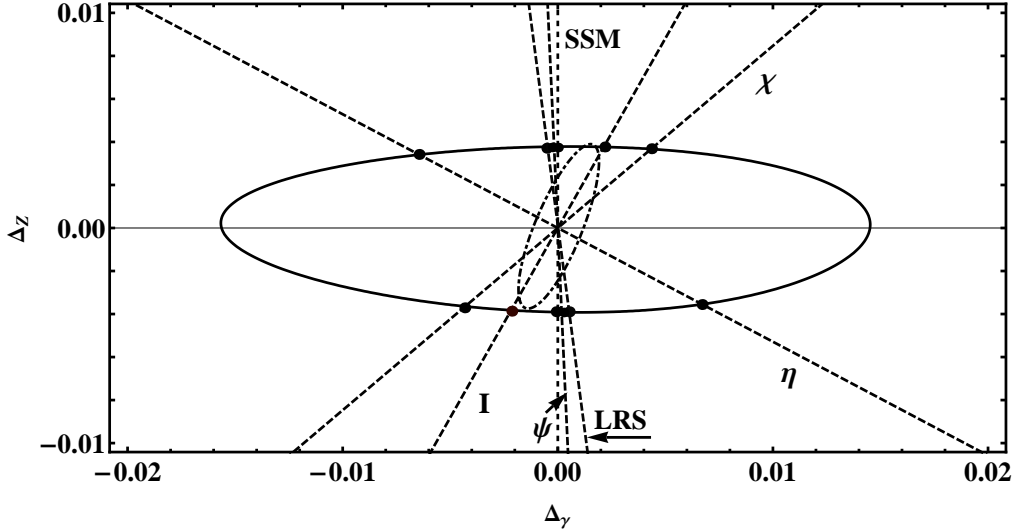


FIG. 8: The outer ellipse (solid) shows the confusion region (95% C.L., see Eq. (37)) in the parameter plane $(\Delta_\gamma, \Delta_Z)$, outside of which a generic Z' model can be identified against an AGC model with non-vanishing parameter x_γ . Polarized cross section with $P_L = \pm 0.8$ and $\bar{P}_L = \mp 0.5$ are assumed. The dashed inner ellipse reproduces the discovery reach on the Z' of Fig. 7, corresponding to $x_\gamma = 0$ in Eq. (37), where the AGC model coincides with the SM. The dashed straight lines correspond to specific extended gauge models (χ , ψ , η , I and LRS). Here, $\sqrt{s} = 0.5$ TeV and $\mathcal{L}_{\text{int}} = 500 \text{ fb}^{-1}$.

confusion region, onto the plane $(\Delta_\gamma, \Delta_Z)$. Any determination of Δ_γ and Δ_Z in the planar domain exterior to the ellipse would allow both Z' discovery and identification against the x_γ -AGC model. Similar to the case of discovery, also in the case of Z' identification the bounds on Δ_γ and Δ_Z could be translated into limits on the Z - Z' mixing angle ϕ and mass M_2 for any specific Z' model.

The procedure outlined above can be repeated for all other types of models with AGC parameters $(\delta_Z, x_Z, y_\gamma, y_Z)$, and consequently one can evaluate the corresponding “confusion regions” in the $(\Delta_\gamma, \Delta_Z)$ parameter plane. The results of this kind of analysis are represented in Fig. 9 displaying the overlap of the confusion regions (95% C.L.) in the parameter plane $(\Delta_\gamma, \Delta_Z)$ for a generic Z' vector model and AGC models with parameters varying one at a time.

The resulting confusion area (obtained from the overlap of all confusion regions) turns out to be open in the vertical direction, i.e., along the Δ_Z axis. The reason is that the Z' model defined by a particular parameter set where $(\Delta_\gamma = 0, \Delta_Z)$ is indistinguishable from

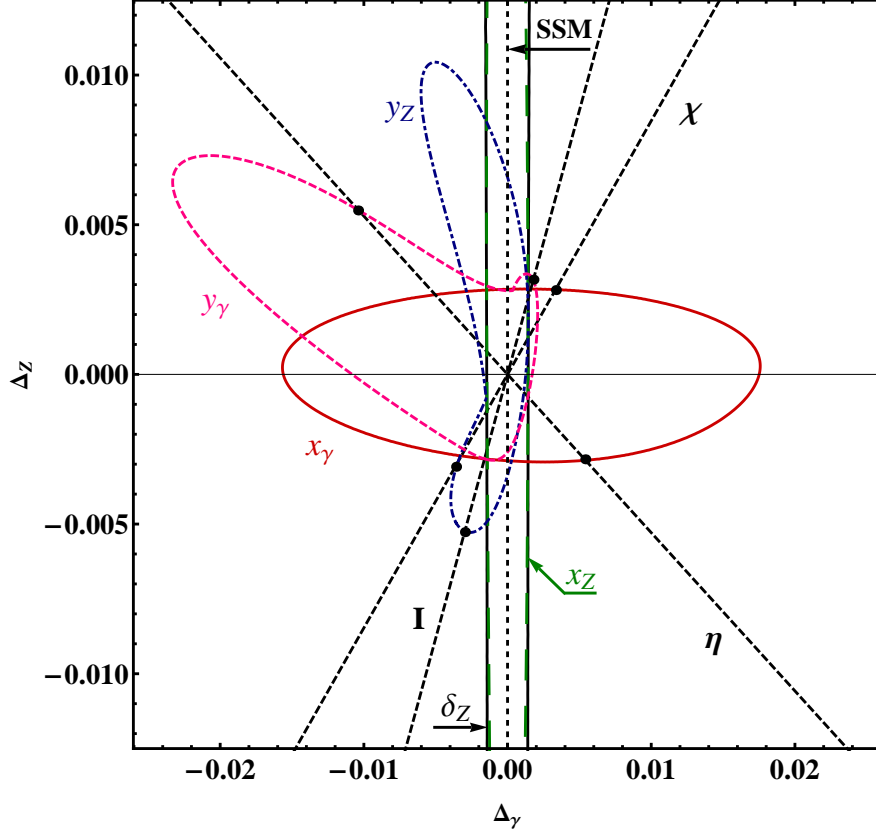


FIG. 9: The closed contours indicate regions of $(\Delta_\gamma, \Delta_Z)$ that can be populated by variations of an AGC parameter, such as for example x_γ . They are thus confusion regions (95%C.L.) in the parameter plane $(\Delta_\gamma, \Delta_Z)$ for a generic Z' model and AGC models with parameters taking non-vanishing values, one at a time: x_γ , x_Z , y_γ , y_Z and δ_Z . Polarized cross sections with $P_L = \pm 0.8$ and $\bar{P}_L = \mp 0.5$ have been exploited. Dashed straight lines correspond to specific Z' models (χ , ψ , η , I and LRS). Here, $\sqrt{s} = 0.5$ TeV and $\mathcal{L}_{\text{int}} = 500 \text{ fb}^{-1}$.

those originating from AGC with the same $\delta_Z = \Delta_Z$. Moreover, from a comparison of the confusion region depicted in Fig. 9 with the corresponding discovery reach presented in Fig. 7 one can conclude that all Z' models might be discovered in the process (1) with polarized beams. However, they may not all be *identified*, the reason being that the confusion region shown in Fig. 9 is not closed, in contrast to the reach shown in Fig. 7.

An example relevant to the current discussion can be found in the SSM model. In fact, from Eq. (35) one can conclude that the signature space of the SSM model in the $(\Delta_\gamma, \Delta_Z)$ parameter plane extends along Δ_Z . It implies that the SSM might be discovered in the process (1) but not separated from AGC models characterized by the parameter Δ_Z . More

generally, those models where the Z' -electron couplings satisfy the equation $v'/a' = v/a$ that, as follows from Eq. (26), lead to $\Delta_\gamma = 0$ can not be distinguished from the AGC case in the W^\pm pair production process. However, all other Z' models (apart from the considered exceptional case) described by the pair of parameters $(\Delta_\gamma, \Delta_Z)$ that are located outside of the confusion area shown in Fig. 9 can be identified. Notice that the above constraint on the electron couplings is fulfilled for an E_6 model at $\beta = 87^\circ$ and for an LRS model with $\alpha_{LR} = 1.36$.

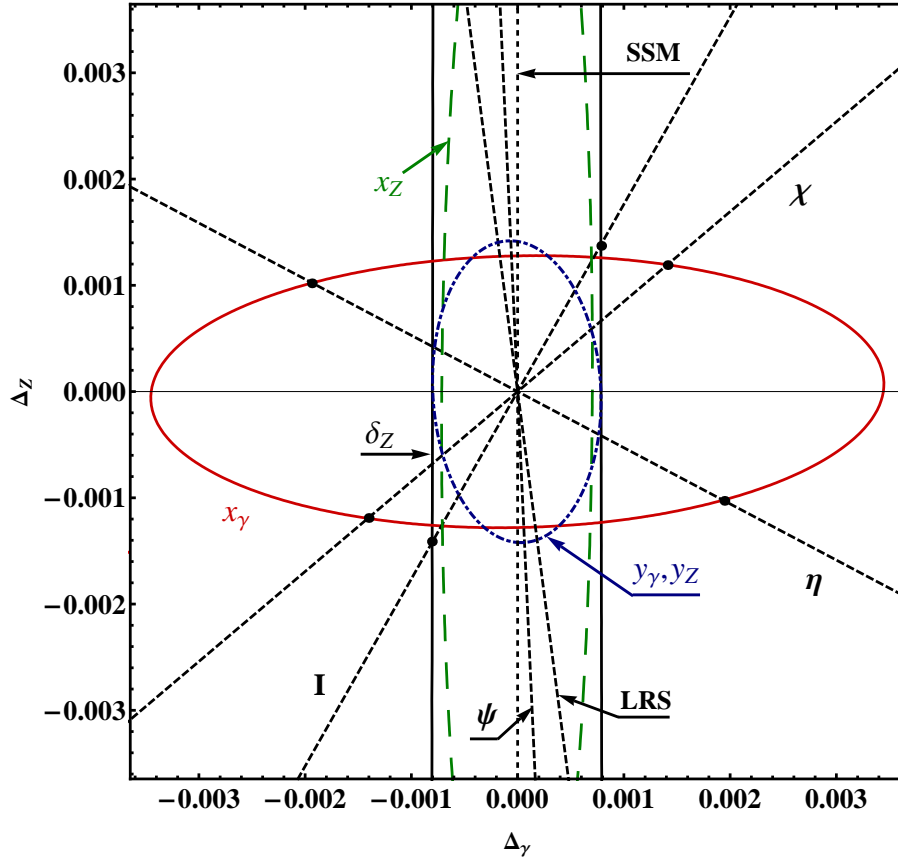


FIG. 10: Same as in Fig. 9 but obtained from combined analysis of the process (1) with polarized initial beams and polarized W^\pm final states. The x_Z contour closes at $\Delta_Z \simeq \pm 0.006$.

The results of a further potential extension of the present analysis are presented in Fig. 10 where the feasibility of measuring polarized W^\pm states in the process (1) is assumed. This assumption is based on the experience gained at LEP2 on measurements of W polarisation [36]. The relevant theoretical framework for measurement of W^\pm polarisation was described in [20, 21]. The method exploited for the measurement of W polarisation is based on the spin density matrix elements that allow to obtain the differential cross sections for polarised

W bosons. Information on spin density matrix elements as functions of the W^- production angle with respect to the electron beam direction was extracted from the decay angles of the charged lepton in the W^- (W^+) rest frame.

B. Model dependent analysis

As mentioned above, the ranges of Δ_γ and Δ_Z allowed to the specific models in Figs. 9 and 10 can be translated into discovery and identification reaches on the mixing angle ϕ and the heavier gauge boson mass M_2 , using Eqs. (26)–(27). The resulting allowed regions, discovery and identification (at the 95% CL) in the (ϕ, M_2) plane is limited in this case by the thick dashed and solid lines, respectively, in Figs. 11– 12 for some specific E_6 models. These limits are obtained from the polarized differential distributions of W with collider energy $\sqrt{s} = 0.5$ TeV and integrated luminosity $\mathcal{L}_{\text{int}} = 500 \text{ fb}^{-1}$. Also, an indicative typical lower bound on M_2 from direct searches at the LHC with $\sqrt{s} = 7$ TeV [9, 10] is reported in these figures as horizontal straight lines. The vertical arrows then indicate the range of available Z' mass values according to LHC limits.

TABLE I: Discovery and identification reach on the Z - Z' mixing angle ϕ for Z' models with $M_2 = 2$ TeV obtained from the polarized differential cross section with ($P_L = \pm 0.8$, $\bar{P}_L = \mp 0.5$) and unpolarized final states for the case $\sqrt{s} = 0.5$ TeV and $\mathcal{L}_{\text{int}} = 500 \text{ fb}^{-1}$. The corresponding limits for polarized W s are given in parenthesis.

Z' model	χ	ψ	η	I	LRS	SSM
$\phi^{\text{DIS}}, 10^{-3}$	$\pm 1.5(0.8)$	$\pm 2.3(1.4)$	$\pm 1.6(1.3)$	$\pm 2.0(0.8)$	$\pm 1.4(1.0)$	$\pm 1.2(0.7)$
$\phi^{\text{ID}}, 10^{-3}$	$\pm 3.8(1.5)$	$\pm 36.8(18.5)$	$\pm 17.4(3.2)$	$\pm 4.3(1.2)$	$\pm 8.1(4.2)$	–

Figures 11 and 12 show that the process $e^+e^- \rightarrow W^+W^-$ at 0.5 TeV has a potential sensitivity to the mixing angle ϕ of the order of 10^{-4} – 10^{-3} or even less, depending on the mass M_2 . This sensitivity would increase for the c.m. energy \sqrt{s} approaching M_2 because the contribution of the Z_2 exchange diagram in Fig. 1 would be enhanced. However, Z' bosons relevant to the extended models under study with mass below $\sim 2.0 - 2.3$ TeV are already excluded by LHC data, and the ILC c.m. energies considered here are therefore

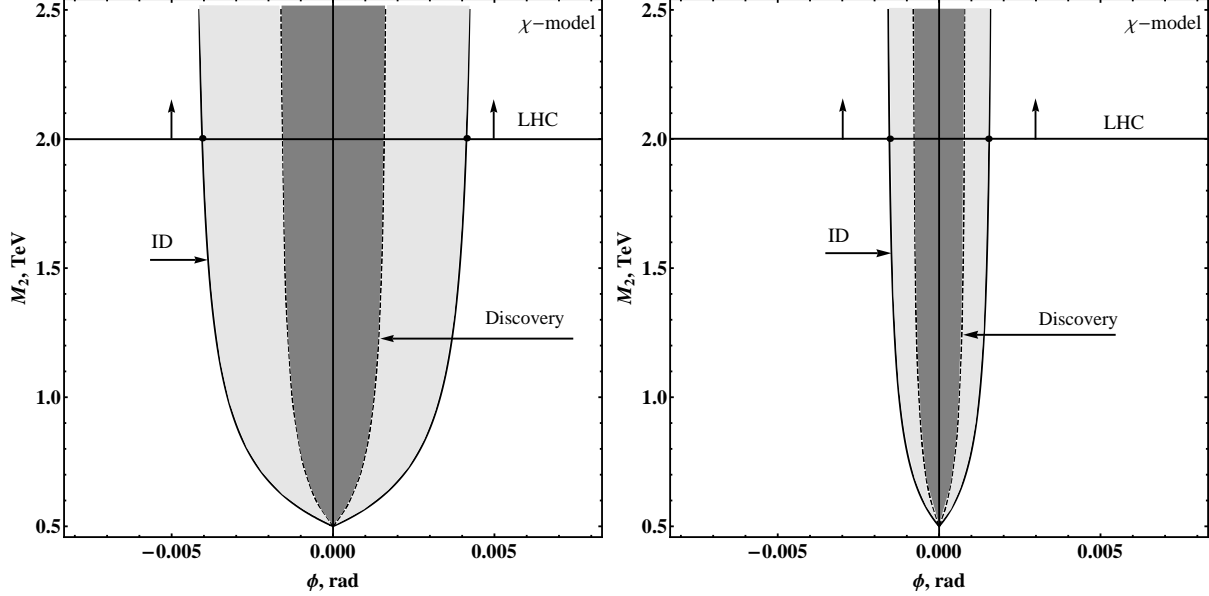


FIG. 11: Left: Discovery (dashed line) and identification (solid line) reach for the χ model in the (ϕ, M_2) plane obtained from polarized initial e^+ and e^- beams with $(P_L = \pm 0.8, \bar{P}_L = \mp 0.5)$ and unpolarized final W^\pm states. Right: The same with polarized final W^\pm states. Here, $\sqrt{s} = 0.5$ TeV and $\mathcal{L}_{\text{int}} = 500 \text{ fb}^{-1}$. The horizontal line with vertical arrows, here and in the next figures, approximately indicates the range of M_2 currently allowed by LHC.

quite far from the admissible M_2 . Conversely, for masses M_2 much larger than \sqrt{s} such that the Z_2 exchange contribution $|\chi_2/\chi|$ is much less than unity, the limiting contour is mostly determined by the modification (10) of the Z couplings to electrons. The discovery and identification reaches on ϕ at $M_2 = 2$ TeV are summarized in Table I.

For the ILC with higher energy and luminosity, $\sqrt{s} = 1$ TeV and $\mathcal{L}_{\text{int}} = 1 \text{ ab}^{-1}$, one expects further improvement of the discovery and identification reach on the Z - Z' mixing angle and M_2 (see Figures 13, 14 and Table II).

TABLE II: Same as in Table I but for ILC with $\sqrt{s} = 1$ TeV and $\mathcal{L}_{\text{int}} = 1 \text{ ab}^{-1}$.

Z' model	χ	ψ	η	I	LRS	SSM
$\phi^{\text{DIS}}, 10^{-4}$	$\pm 3.8(1.8)$	$\pm 5.8(3.4)$	$\pm 4.6(3.2)$	$\pm 4.4(1.9)$	$\pm 3.7(2.4)$	$\pm 3.1(1.7)$
$\phi^{\text{ID}}, 10^{-4}$	$\pm 9.0(4.2)$	$\pm 94(45)$	$\pm 24(9.5)$	$\pm 6.1(2.8)$	$\pm 18(10)$	–

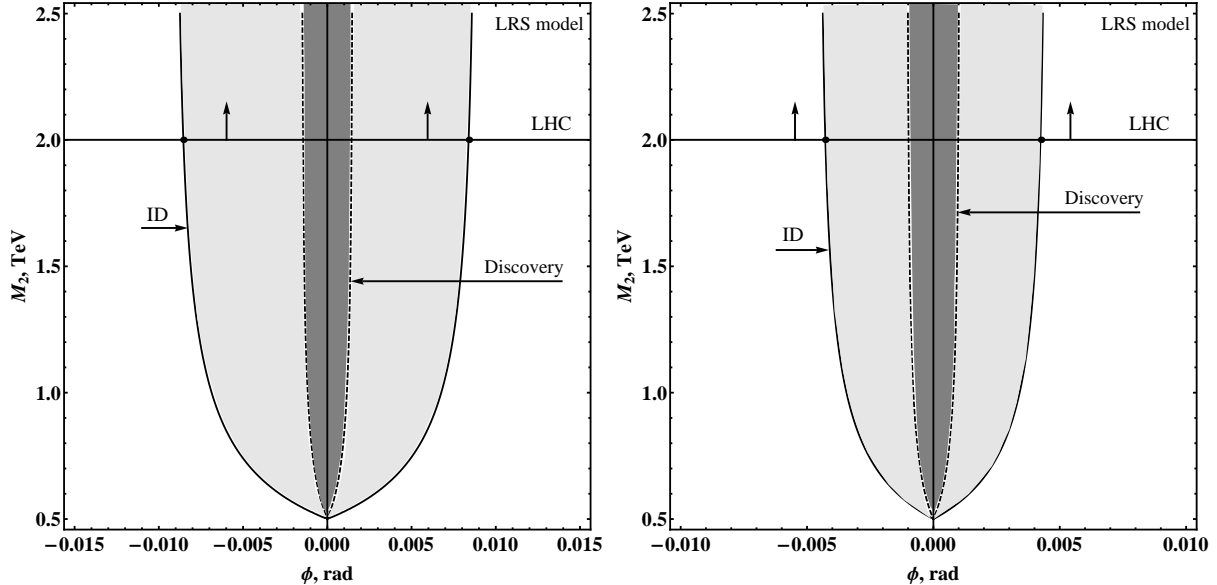


FIG. 12: Same as in Fig.11 but for the LRS model.

As already mentioned, the horizontal lines in Figs. 11–14 denote the current LHC lower limits on M_2 , therefore only the upper parts, as indicated by the vertical arrows, will be available for discovery and identification of a Z' *via* indirect manifestations at the ILC with the considered values for the c.m. energy of 0.5 and 1 TeV. Since those limits are so much higher than \sqrt{s} , the corrections from finite Z' widths, assumed in the range $\Gamma_{Z'} = (0.01–0.10)M_{Z'}$ [1], are found to be numerically negligible in the “working” regions indicated in those figures by the horizontal lines and vertical arrows. Tables I and II demonstrate that ILC (0.5 TeV) and ILC (1 TeV) allow to improve current bounds on Z – Z' mixing for most of the Z' models, and also differentiating Z' from AGC is feasible.

C. Low-energy option

Currently, physics at the ILC in a low-energy option is extensively studied and discussed, as it in this mode might act as a “Higgs factory”. The results for discovery and identification reach on Z – Z' mixing and mass M_2 obtained from the ILC with $\sqrt{s} = 0.25$ TeV and 0.35 TeV are summarized in Tables III and IV.

The comparison of these constraints with those obtained from electroweak precision data derived mostly from on- Z -resonance experiments at LEP1 and SLC [7] shows that the ILC (0.25 TeV) and ILC (0.35 TeV) allow to obtain bounds on Z – Z' mixing at the same

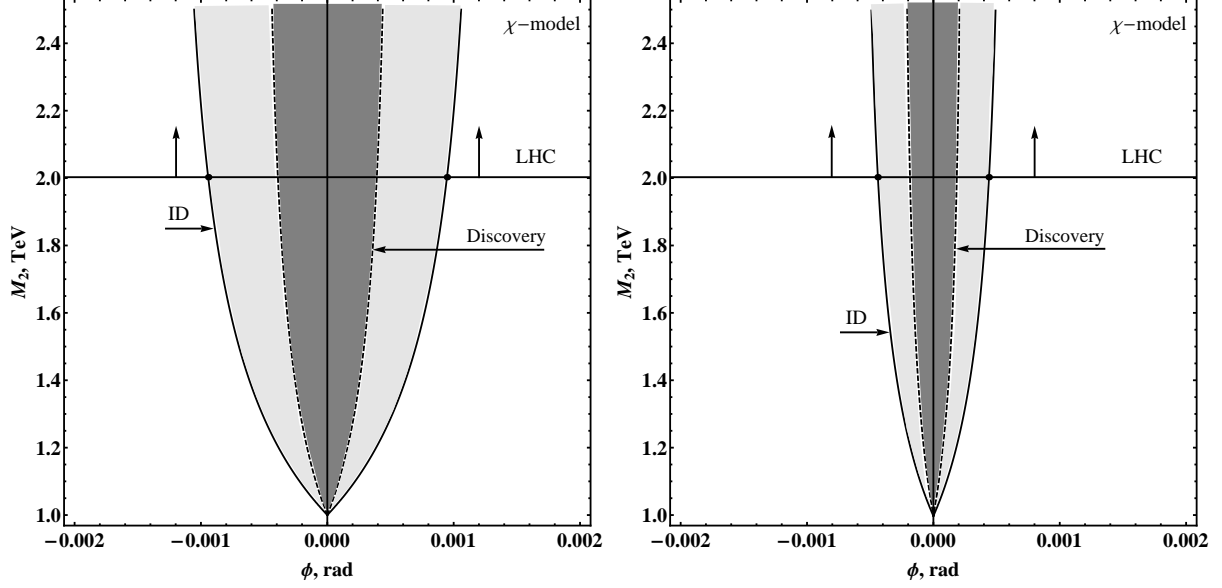


FIG. 13: Left: Discovery (dashed line) and identification (solid line) reach for the χ model in the (ϕ, M_2) plane obtained from polarized initial e^+ and e^- beams with $(P_L = \pm 0.8, \bar{P}_L = \mp 0.5)$ and unpolarized final W^\pm states. Right: The same with polarized final W^\pm states. Here, $\sqrt{s} = 1$ TeV and $\mathcal{L}_{\text{int}} = 1 \text{ ab}^{-1}$.

TABLE III: Same as in Table I but for the ILC with $\sqrt{s} = 0.25$ TeV and $\mathcal{L}_{\text{int}} = 100 \text{ fb}^{-1}$.

Z' model	χ	ψ	η	I	LRS	SSM
$\phi^{\text{DIS}}, 10^{-3}$	$\pm 5.1(3.8)$	$\pm 8.4(7.0)$	$\pm 6.8(6.7)$	$\pm 5.7(3.9)$	$\pm 5.4(4.9)$	$\pm 4.4(3.6)$
$\phi^{\text{ID}}, 10^{-3}$	$\pm 14(6.8)$	$\pm 109(86)$	$\pm 29(14)$	$\pm 7.8(5.9)$	$\pm 45(21)$	–

level as those of current experimental limits, thereby providing complementary bounds on Z' s.

Increasing the luminosity at fixed energy, asymptotically allows for an increase of the sensitivity $\propto 1/\sqrt{\mathcal{L}_{\text{int}}}$. In the example shown in Table IV, this behavior is not quite reached, due to the impact of systematic uncertainties.

VII. CONCLUDING REMARKS

We have discussed the foreseeable sensitivity to Z' s in W^\pm -pair production cross sections at the ILC, especially as regards the potential of distinguishing observable effects of a Z' from

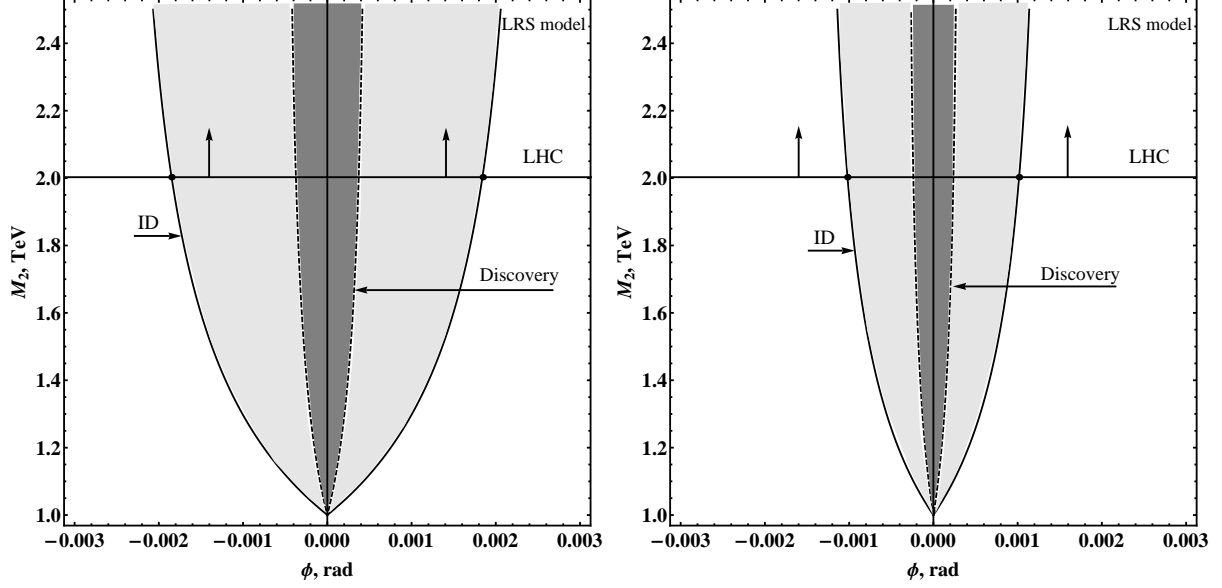


FIG. 14: Same as in Fig.13 but for the LRS model.

TABLE IV: Same as in Table III but for the ILC with $\sqrt{s} = 0.35$ TeV, and two values of integrated luminosity.

Z' model		χ	ψ	η	I	LRS	SSM
100 fb^{-1}	$\phi^{\text{DIS}}, 10^{-3}$	$\pm 3.7(2.4)$	$\pm 6.0(4.5)$	$\pm 4.9(4.3)$	$\pm 4.1(2.5)$	$\pm 3.9(3.1)$	$\pm 3.2(2.3)$
	$\phi^{\text{ID}}, 10^{-3}$	$\pm 8.4(4.6)$	$\pm 77(61)$	$\pm 27(9.4)$	$\pm 13.5(3.8)$	$\pm 19(14)$	–
500 fb^{-1}	$\phi^{\text{DIS}}, 10^{-3}$	$\pm 2.3(1.3)$	$\pm 3.4(2.3)$	$\pm 2.5(2.1)$	$\pm 3.1(1.4)$	$\pm 2.1(1.6)$	$\pm 1.8(1.2)$
	$\phi^{\text{ID}}, 10^{-3}$	$\pm 5.9(2.4)$	$\pm 54(30)$	$\pm 15(4.7)$	$\pm 4.0(1.9)$	$\pm 16(6.8)$	–

analogous ones due to competitor models with Anomalous Gauge Couplings that can lead to the same or similar new physics experimental signatures. The discovery and identification reaches on E_6 and LRS models have been determined in the parameter plane spanned by the Z - Z' mixing angle ϕ , and Z' mass, M_2 .

We have shown that the sensitivity of the ILC for probing the Z - Z' mixing and its capability to distinguish these two new physics scenarios is substantially enhanced when the polarization of the initial beams (and also, possibly, the produced W^\pm bosons) are considered.

Acknowledgements

It is a pleasure to thank S. Dittmaier for valuable comments on the importance of the radiative corrections. This research has been partially supported by the Abdus Salam ICTP under the TRIL and STEP Programmes and the Belarusian Republican Foundation for Fundamental Research. The work of AAP has been partially supported by the SFB 676 Programme of the Department of Physics, University of Hamburg. The work of PO has been supported by the Research Council of Norway.

Appendix A. Helicity amplitudes

In this appendix, we collect the helicity amplitudes for the different initial (e^+e^-) and final-state (W^+W^-) polarizations. In Table V we quote the amplitudes for the case of Anomalous Gauge Couplings [20, 21], whereas in Table VI we give the corresponding results for the case of a Z' .

Note that the quantity δ_Z appearing in Table V is different from, but plays a role similar to that of Δ_Z entering in the parametrization of Z' effects. Furthermore, in analogy with the Δ_γ which enters the description of Z' effects, one could imagine a factor $(1 + \delta_\gamma)$ multiplying the photon-exchange amplitudes in Table V. Such a term could be induced by dimension-8 operators, but δ_γ would have to vanish as $s \rightarrow 0$, due to gauge invariance.

TABLE V: Helicity amplitudes for $e^+e^- \rightarrow W^+W^-$ in the presence of AGC [20, 21]. To obtain the amplitude $F_{\lambda\tau\tau'}(s, \cos\theta)$ for definite helicity $\lambda = \pm 1/2$ and definite spin orientations $\tau(W^-)$ and $\tau'(W^+)$ of the W^\pm , the elements in the corresponding column have to be multiplied by the common factor on top of the column. Subsequently, the elements in a specific column have to be multiplied by the corresponding elements in the first column and the sum over all elements is to be taken. In the last column, the amplitude for the case of $\tau = \pm 1, \tau' = 0$ is obtained by replacing τ' by $-\tau$ in the elements of this last column.

$e_{-\lambda}^+ e_{\lambda}^- \rightarrow W_L^+ W_L^-$	$\tau = \tau' = 0$ $-\frac{e^2 s \lambda}{2} \sin \theta$	
$\frac{2\lambda-1}{4t s_W^2}$	$\frac{s}{2M_W^2} [\cos \theta - \beta_W (1 + \frac{2M_W^2}{s})]$	
$-\frac{2}{s} + \frac{2(\cot \theta_W + \delta_Z)}{s-M_Z^2} (v-2a\lambda)$	$-\beta_W (1 + \frac{s}{2M_W^2})$	
$-\frac{x_\gamma}{s} + \frac{x_Z}{s-M_Z^2} (v-2a\lambda)$	$-\beta_W \frac{s}{M_W^2}$	
$e_{-\lambda}^+ e_{\lambda}^- \rightarrow W_T^+ W_T^-$	$\tau = \tau' = \pm 1$ $-\frac{e^2 s \lambda}{2} \sin \theta$	$\tau = -\tau' = \pm 1$ $-\frac{e^2 s \lambda}{2} \sin \theta$
$\frac{2\lambda-1}{4t s_W^2}$	$\cos \theta - \beta_W$	$-\cos \theta - 2\tau\lambda$
$-\frac{2}{s} + \frac{2(\cot \theta_W + \delta_Z)}{s-M_Z^2} (v-2a\lambda)$	$-\beta_W$	0
$-\frac{y_\gamma}{s} + \frac{y_Z}{s-M_Z^2} (v-2a\lambda)$	$-\beta_W \frac{s}{M_W^2}$	0
$e_{-\lambda}^+ e_{\lambda}^- \rightarrow W_T^+ W_L^-$	$\tau = 0, \tau' = \pm 1$ $-\frac{e^2 s \lambda}{2\sqrt{2}} (\tau' \cos \theta - 2\lambda)$	$\tau = \pm 1, \tau' = 0$ $\frac{e^2 s \lambda}{2\sqrt{2}} (\tau \cos \theta + 2\lambda)$
$\frac{2\lambda-1}{4t s_W^2}$	$\frac{\sqrt{s}}{2M_W} [\cos \theta (1 + \beta_W^2) - 2\beta_W]$ $-\frac{2M_W}{\sqrt{s}} \frac{\tau' \sin^2 \theta}{\tau' \cos \theta - 2\lambda}$	$\frac{\sqrt{s}}{2M_W} [\cos \theta (1 + \beta_W^2) - 2\beta_W]$ $-\frac{2M_W}{\sqrt{s}} \frac{\tau \sin^2 \theta}{\tau \cos \theta + 2\lambda}$
$-\frac{2}{s} + \frac{2(\cot \theta_W + \delta_Z)}{s-M_Z^2} (v-2a\lambda)$	$-\beta_W \frac{\sqrt{s}}{M_W}$	$-\beta_W \frac{\sqrt{s}}{M_W}$
$-\frac{x_\gamma + y_\gamma}{s} + \frac{x_Z + y_Z}{s-M_Z^2} (v-2a\lambda)$	$-\beta_W \frac{\sqrt{s}}{M_W}$	$-\beta_W \frac{\sqrt{s}}{M_W}$

TABLE VI: Helicity amplitudes for $e^+e^- \rightarrow \gamma, Z_1, Z_2 \rightarrow W^+W^-$.

$e_{-\lambda}^+ e_{\lambda}^- \rightarrow W_L^+ W_L^-$	$\tau = \tau' = 0$ $-\frac{e^2 s \lambda}{2} \sin \theta$	
$\frac{2\lambda-1}{4t s_W^2}$	$\frac{s}{2M_W^2} [\cos \theta - \beta_W (1 + \frac{2M_W^2}{s})]$	
$-\frac{2}{s} + \frac{2g_{WWZ_1}}{s-M_1^2+iM_1\Gamma_1} (v_1 - 2a_1\lambda)$ $+\frac{2g_{WWZ_2}}{s-M_2^2+iM_2\Gamma_2} (v_2 - 2a_2\lambda)$ $\approx -\frac{2(1+\Delta\gamma)}{s} + \frac{2(\cot\theta_W+\Delta Z)}{s-M_Z^2} (v - 2a\lambda)$	$-\beta_W (1 + \frac{s}{2M_W^2})$	
$e_{-\lambda}^+ e_{\lambda}^- \rightarrow W_T^+ W_T^-$	$\tau = \tau' = \pm 1$ $-\frac{e^2 s \lambda}{2} \sin \theta$	$\tau = -\tau' = \pm 1$ $-\frac{e^2 s \lambda}{2} \sin \theta$
$\frac{2\lambda-1}{4t s_W^2}$	$\cos \theta - \beta_W$	$-\cos \theta - 2\tau\lambda$
$-\frac{2}{s} + \frac{2g_{WWZ_1}}{s-M_1^2+iM_1\Gamma_1} (v_1 - 2a_1\lambda)$ $+\frac{2g_{WWZ_2}}{s-M_2^2+iM_2\Gamma_2} (v_2 - 2a_2\lambda)$ $\approx -\frac{2(1+\Delta\gamma)}{s} + \frac{2(\cot\theta_W+\Delta Z)}{s-M_Z^2} (v - 2a\lambda)$	$-\beta_W$	0
$e_{-\lambda}^+ e_{\lambda}^- \rightarrow W_T^+ W_L^-$	$\tau = 0, \tau' = \pm 1$ $-\frac{e^2 s \lambda}{2\sqrt{2}} (\tau' \cos \theta - 2\lambda)$	$\tau = \pm 1, \tau' = 0$ $\frac{e^2 s \lambda}{2\sqrt{2}} (\tau \cos \theta + 2\lambda)$
$\frac{2\lambda-1}{4t s_W^2}$	$\frac{\sqrt{s}}{2M_W} [\cos \theta (1 + \beta_W^2) - 2\beta_W]$ $-\frac{2M_W}{\sqrt{s}} \frac{\tau' \sin^2 \theta}{\tau' \cos \theta - 2\lambda}$	$\frac{\sqrt{s}}{2M_W} [\cos \theta (1 + \beta_W^2) - 2\beta_W]$ $-\frac{2M_W}{\sqrt{s}} \frac{\tau \sin^2 \theta}{\tau \cos \theta + 2\lambda}$
$-\frac{2}{s} + \frac{2g_{WWZ_1}}{s-M_1^2+iM_1\Gamma_1} (v_1 - 2a_1\lambda)$ $+\frac{2g_{WWZ_2}}{s-M_2^2+iM_2\Gamma_2} (v_2 - 2a_2\lambda)$ $\approx -\frac{2(1+\Delta\gamma)}{s} + \frac{2(\cot\theta_W+\Delta Z)}{s-M_Z^2} (v - 2a\lambda)$	$-\beta_W \frac{\sqrt{s}}{M_W}$	$-\beta_W \frac{\sqrt{s}}{M_W}$

-
- [1] P. Langacker, Rev. Mod. Phys. **81**, 1199-1228 (2009) [arXiv:0801.1345 [hep-ph]].
- [2] T. G. Rizzo, [hep-ph/0610104].
- [3] A. Leike and S. Riemann, Z. Phys. C **75**, 341 (1997) [hep-ph/9607306].
- [4] A. Leike, Phys. Rept. **317**, 143-250 (1999) [hep-ph/9805494].
- [5] S. Riemann, eConf C **050318**, 0303 (2005) [hep-ph/0508136].
- [6] J. L. Hewett, T. G. Rizzo, Phys. Rept. **183**, 193 (1989).
- [7] J. Erler, P. Langacker, S. Munir, E. Rojas, JHEP **0908**, 017 (2009) [arXiv:0906.2435 [hep-ph]].
- [8] P. Langacker, [arXiv:0911.4294 [hep-ph]].
- [9] S. Chatrchyan *et al.* [CMS Collaboration], Phys. Lett. **B714**, 158-179 (2012) [arXiv:1206.1849 [hep-ex]].
- [10] ATLAS Collaboration, Note ATLAS-CONF-2012-007 (March 2012).
- [11] P. Osland, A. A. Pankov, A. V. Tsytrinov, N. Paver, Phys. Rev. **D79**, 115021 (2009) [arXiv:0904.4857 [hep-ph]].
- [12] J. Brau *et al.* [ILC Collaboration], "ILC Reference Design Report Volume 1 - Executive Summary," arXiv:0712.1950 [physics.acc-ph].
- [13] G. Aarons *et al.* [ILC Collaboration], "International Linear Collider Reference Design Report Volume 2: PHYSICS AT THE ILC," arXiv:0709.1893 [hep-ph].
- [14] A. A. Pankov, N. Paver, Phys. Lett. **B272**, 425-430 (1991).
- [15] A. A. Pankov, N. Paver, Phys. Rev. **D48**, 63-77 (1993).
- [16] A. A. Pankov, N. Paver, Phys. Lett. **B324**, 224-230 (1994).
- [17] A. A. Pankov, N. Paver, C. Verzegnassi, Int. J. Mod. Phys. **A13**, 1629-1650 (1998) [hep-ph/9701359].
- [18] D. -W. Jung, K. Y. Lee, H. S. Song, C. Yu, J. Korean Phys. Soc. **36**, 258-264 (2000) [hep-ph/9905353].
- [19] B. Ananthanarayan, M. Patra, P. Poulose, JHEP **1102**, 043 (2011) [arXiv:1012.3566 [hep-ph]].
- [20] G. Gounaris, J. L. Kneur, J. Layssac, G. Moulataka, F. M. Renard and D. Schildknecht, Proceedings of the Workshop *e⁺e⁻ Collisions at 500 GeV: the Physics Potential*, Ed. P.M. Zerwas (1992), DESY 92-123B, p.735.
- [21] G. Gounaris, J. Layssac, G. Moulataka, F. M. Renard, Int. J. Mod. Phys. **A8**, 3285-3320 (1993).

- [22] G. Moortgat-Pick, T. Abe, G. Alexander, B. Ananthanarayan, A. A. Babich, V. Bharadwaj, D. Barber, A. Bartl *et al.*, Phys. Rept. **460**, 131-243 (2008) [hep-ph/0507011].
- [23] P. Osland, A. A. Pankov, A. V. Tsytrinov, Eur. Phys. J. **C67**, 191-204 (2010) [arXiv:0912.2806 [hep-ph]].
- [24] P. Langacker and M. -x. Luo, Phys. Rev. D **45**, 278 (1992).
- [25] K. Hagiwara, R. D. Peccei, D. Zeppenfeld and K. Hikasa, Nucl. Phys. B **282**, 253 (1987)
- [26] M. S. Bilenky, J. L. Kneur, F. M. Renard and D. Schildknecht, Nucl. Phys. B **409**, 22 (1993).
- [27] M. S. Bilenky, J. L. Kneur, F. M. Renard and D. Schildknecht, Nucl. Phys. B **419**, 240 (1994) [hep-ph/9312202].
- [28] K. Nakamura *et al.* [Particle Data Group Collaboration], J. Phys. G **37**, 075021 (2010).
- [29] J. Fleischer, K. Kolodziej and F. Jegerlehner, Phys. Rev. D **47**, 830 (1993).
- [30] W. Beenakker and A. Denner, Int. J. Mod. Phys. A **9**, 4837 (1994).
- [31] A. Denner, S. Dittmaier, M. Roth and L. H. Wieders, Phys. Lett. B **612**, 223 (2005) [Erratum-
ibid. B **704**, 667 (2011)] [hep-ph/0502063].
- [32] A. Denner, S. Dittmaier, M. Roth and L. H. Wieders, Nucl. Phys. B **724**, 247 (2005) [Erratum-
ibid. B **854**, 504 (2012)] [hep-ph/0505042].
- [33] W. Beenakker, F. A. Berends and T. Sack, Nucl. Phys. B **367**, 287 (1991).
- [34] W. Beenakker, K. Kolodziej and T. Sack, Phys. Lett. B **258**, 469 (1991).
- [35] A. A. Pankov, N. Paver and A. V. Tsytrinov, Phys. Rev. D **73**, 115005 (2006) [arXiv:hep-ph/0512131].
- [36] G. Abbiendi *et al.*, [OPAL collaboration], Phys. Lett. **B585**, 223 (2004);
P. Achard *et al.*, [L3 collaboration], Phys. Lett. **B557**, 147 (2003);
J. Abdallah *et al.*, [DELPHI Collaboration], Eur. Phys. J. C **54**, 345 (2008) [arXiv:0801.1235 [hep-ex]];
J.P. Couchman, A measurement of the triple gauge boson couplings and W boson polarisation in W -pair production at LEP2, Ph.D. thesis, University College London, 2000.